

$B \rightarrow \phi K_S$   $CP$  asymmetries as a probe of supersymmetry\*Jae-hyeon Park<sup>†</sup>Department of Physics, KAIST  
Daejeon 305-701, Korea

We consider sparticle contributions to time dependent  $CP$  asymmetry in  $B \rightarrow \phi K_S$ . As for the gluino-squark loop,  $LR$  or  $RL$  insertion is more likely to give recently observed  $S_{\phi K} < 0$  than  $LL$  or  $RR$  insertion. Neutral Higgs contribution does not change  $S_{\phi K}$  very much due to the strong constraint from  $B_s \rightarrow \mu^+ \mu^-$ . We also show correlations among related processes such as direct  $CP$  asymmetry in  $B \rightarrow X_s \gamma$  and  $B_s - \bar{B}_s$  mixing, and discuss theoretical motivations for desired strength of flavor violation.

Time dependent  $CP$  asymmetry in  $B \rightarrow \phi K_S$  mode is written as

$$\begin{aligned} \mathcal{A}_{\phi K}(t) &\equiv \frac{\Gamma(\bar{B}^0(t) \rightarrow \phi K_S) - \Gamma(B^0(t) \rightarrow \phi K_S)}{\Gamma(\bar{B}^0(t) \rightarrow \phi K_S) + \Gamma(B^0(t) \rightarrow \phi K_S)} \\ &= -C_{\phi K} \cos(\Delta m_d t) + S_{\phi K} \sin(\Delta m_d t), \end{aligned}$$

where  $\Delta m_d$  denotes the mass splitting between the two mass eigenstates composed of  $B^0$  and  $\bar{B}^0$ . Current data on the coefficients of the sine and cosine terms and their Standard Model (SM) predictions are summarized in Table I. It shows a  $2.7\sigma$  discrepancy between the measured value and SM prediction of  $S_{\phi K}$ . This has become a hot issue in the high energy physics community recently. One of the reasons why physicists are focusing on  $B \rightarrow \phi K_S$  mode is that it is loop suppressed in the SM because it is a purely flavor changing neutral current (FCNC) process. This means that it is more sensitive to possible new physics effects which presumably arise at loop level, than those processes that have tree level contribution such as  $B \rightarrow J/\psi K_S$ . In this work, we consider a possibility of filling this gap between the data and SM value, with effects from supersymmetry (SUSY).

One major source of flavor violation in the general minimal supersymmetric standard model (MSSM) is non-diagonal squark mass matrix. An off-diagonal element in the squark mass matrix in the super CKM basis can constitute a diagram leading to  $b \rightarrow s \bar{q} q$  through gluino

	$S_{\phi K}$	$C_{\phi K}$
BaBar[1]	$+0.45 \pm 0.43 \pm 0.07$	$-0.38 \pm 0.37 \pm 0.12$
Belle[2]	$-0.96 \pm 0.50^{+0.09}_{-0.11}$	$+0.15 \pm 0.29 \pm 0.07$
Average	$-0.15 \pm 0.33$	$-0.05 \pm 0.24$
SM	$0.734 \pm 0.054$	0
Avg. - SM	$-2.7\sigma$	$-0.2\sigma$

TABLE I: Current status of time dependent  $CP$  asymmetry in  $B \rightarrow \phi K_S$ .

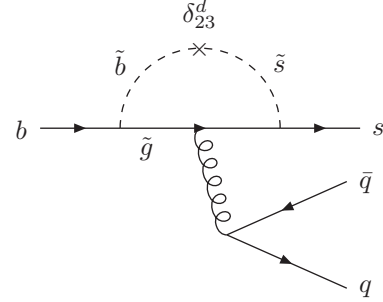


FIG. 1: Gluino-squark loop penguin diagram.

mediation, where  $q = u, d, s, c, b$ . An example of this type of QCD penguin diagram is shown in Fig. 1. Here we adopt the mass insertion (MI) approximation which is one of the most convenient ways to analyzing this type of contribution. We consider four MI's relevant to  $b \rightarrow s$  transitions, i.e.,  $(\delta_{LL}^d)_{23}$ ,  $(\delta_{RR}^d)_{23}$ ,  $(\delta_{LR}^d)_{23}$ , and  $(\delta_{RL}^d)_{23}$ , one at a time. In addition to these four cases, we include another one called  $RL$  dominance scenario [3]. In this case,  $C_{7\gamma}$  and  $C_{8g}$  are assumed to vanish at the  $m_b$  scale, so the observed decay of  $B \rightarrow X_s \gamma$  must come from  $\tilde{C}_{7\gamma}$ , the chirality-flipped version of  $C_{7\gamma}$ . This unconventional scenario and the usual case can be distinguished by measuring the photon polarization. Therefore  $(\delta_{RL}^d)_{23}$  is forced to be a finite size to account for the data unlike the other four cases, and this corresponds to an extreme case with maximized SUSY effect in some sense. In the following, we turn on one of the four MI parameters at a time, and scan over it imposing constraints from  $B \rightarrow X_s \gamma$  and  $B_s - \bar{B}_s$  mixing as follows:

$$\begin{aligned} 2.0 \times 10^{-4} &< B(B \rightarrow X_s \gamma) < 4.5 \times 10^{-4}, \\ \Delta M_s &> 14.9 \text{ ps}^{-1} [4]. \end{aligned}$$

We impose a rather generous bound on  $B(B \rightarrow X_s \gamma)$  to take into account theoretical uncertainties. The common squark mass  $\tilde{m}$  and the gluino mass  $m_{\tilde{g}}$  are chosen to be  $m_{\tilde{g}} = \tilde{m} = 400 \text{ GeV}$ . We use QCD factorization [5] in evaluating hadronic matrix elements for  $B \rightarrow \phi K_S$ . We do not assume any new physics in the  $B^0 - \bar{B}^0$  mixing because  $\sin 2\beta$  measurement from the  $B \rightarrow J/\psi K_S$  mode is well consistent with the SM fit.

\*Talk presented at ICFP2003, Seoul, Oct 6–11, 2003, to appear in the proceedings.

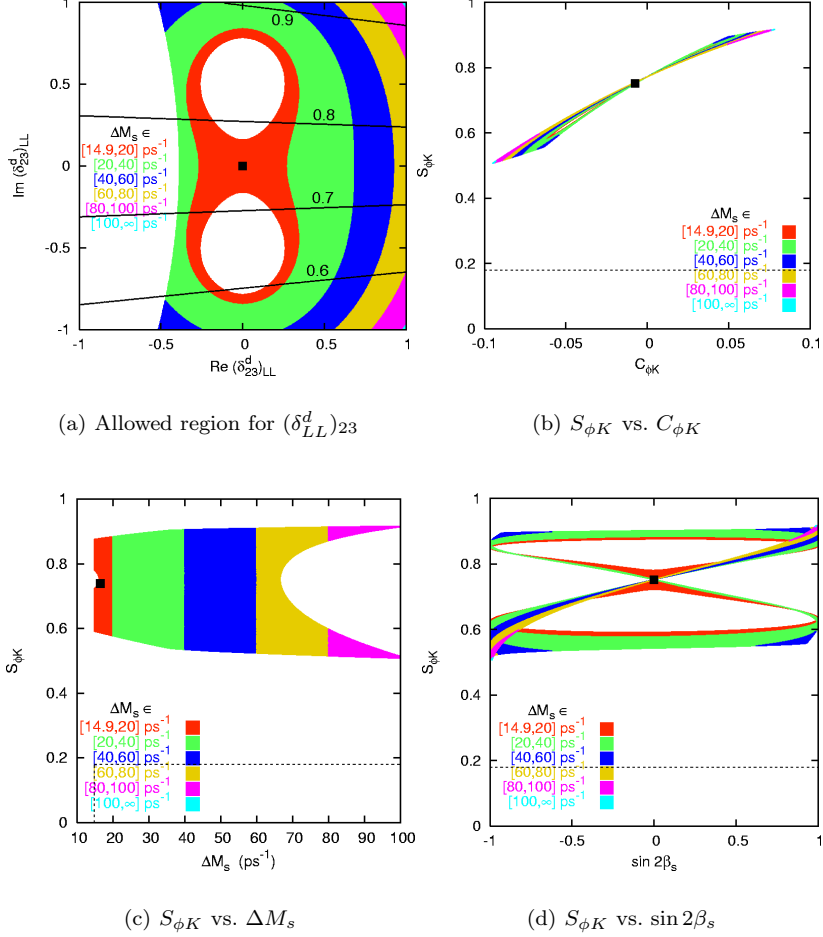


FIG. 2: (a) Allowed region on the complex plane of  $(\delta_{LL}^d)_{23}$ , and (b–d) correlations among observables for the  $LL$  insertion case. Different shades are used for different values of  $\Delta M_s$ . The black square corresponds to the SM case. The dotted line represents the upper bound on  $S_{\phi K}$  at 1- $\sigma$  level. Lines in Fig. (a) are contours of  $S_{\phi K}$ .

First, let us consider the  $LL$  insertion case. Fig. 2 (a) is the region of  $(\delta_{LL}^d)_{23}$  consistent with  $B(B \rightarrow X_s \gamma)$  and  $\Delta M_s$  constraints. The solid lines are contours of  $S_{\phi K}$ . The small square at the origin corresponds to the SM case, because there is no SUSY contribution there. The white space on the left is excluded by too small value of  $B(B \rightarrow X_s \gamma)$ . The two holes around the  $\text{Re}(\delta_{LL}^d)_{23} = 0$  line are excluded by too small  $\Delta M_s$ . In Fig. 2 (b), we plot predictions of  $S_{\phi K}$  and  $C_{\phi K}$  from the allowed values of  $(\delta_{LL}^d)_{23}$ . The dotted horizontal line is the current 1- $\sigma$  upper limit on  $S_{\phi K}$ . This figure shows that the minimal value of  $S_{\phi K}$  in this case is about +0.5, and the change of  $S_{\phi K}$  from the SM prediction is not significant. Although  $S_{\phi K}$  is not very much affected, large effect in  $B_s - \overline{B}_s$  can be expected. For example, we show the prediction of  $\Delta M_s$  in Fig. 2 (c). The SM value of  $\Delta M_s$  is about 16 ps<sup>-1</sup>, marked by the black square. We can read huge enhancement of  $\Delta M_s \sim 50$  ps<sup>-1</sup> is possible. Also, we show  $\sin 2\beta_s$  in Fig. 2 (d), where  $2\beta_s$  is the phase of

$\langle B_s | H_{\text{eff}}^{\Delta B=2} | \overline{B}_s \rangle$ . The SM prediction of it is almost zero, but it can have any value between  $-1$  and  $1$  here, which means that  $CP$  violation in  $B_s - \overline{B}_s$  mixing can drastically change.

The  $RR$  insertion case is almost identical to the  $LL$  insertion case. The only difference is the way  $B(B \rightarrow X_s \gamma)$  constrains  $(\delta_{RR}^d)_{23}$ . The  $LL$  ( $RR$ ) insertion mainly contributes to  $C_{7\gamma}$  ( $\tilde{C}_{7\gamma}$ ), and the dependence is such that

$$B(B \rightarrow X_s \gamma) \propto |C_{7\gamma}^{\text{SM}} + C_{7\gamma}^{\text{SUSY}}|^2, \quad \text{for } LL,$$

$$B(B \rightarrow X_s \gamma) \propto |C_{7\gamma}^{\text{SM}}|^2 + |\tilde{C}_{7\gamma}^{\text{SUSY}}|^2, \quad \text{for } RR.$$

Because of this difference,  $(\delta_{RR}^d)_{23}$  plane does not show a region excluded by  $B(B \rightarrow X_s \gamma)$  that is present in Fig. 2 (a). However, this additional parameter space does not help shifting down  $S_{\phi K}$  very much. Plots for this case are available in Ref. [6].

It is well known that the chirality-flipping  $LR$  and  $RL$  insertions receive enhancement by the factor of  $m_{\tilde{g}}/m_b$ ,

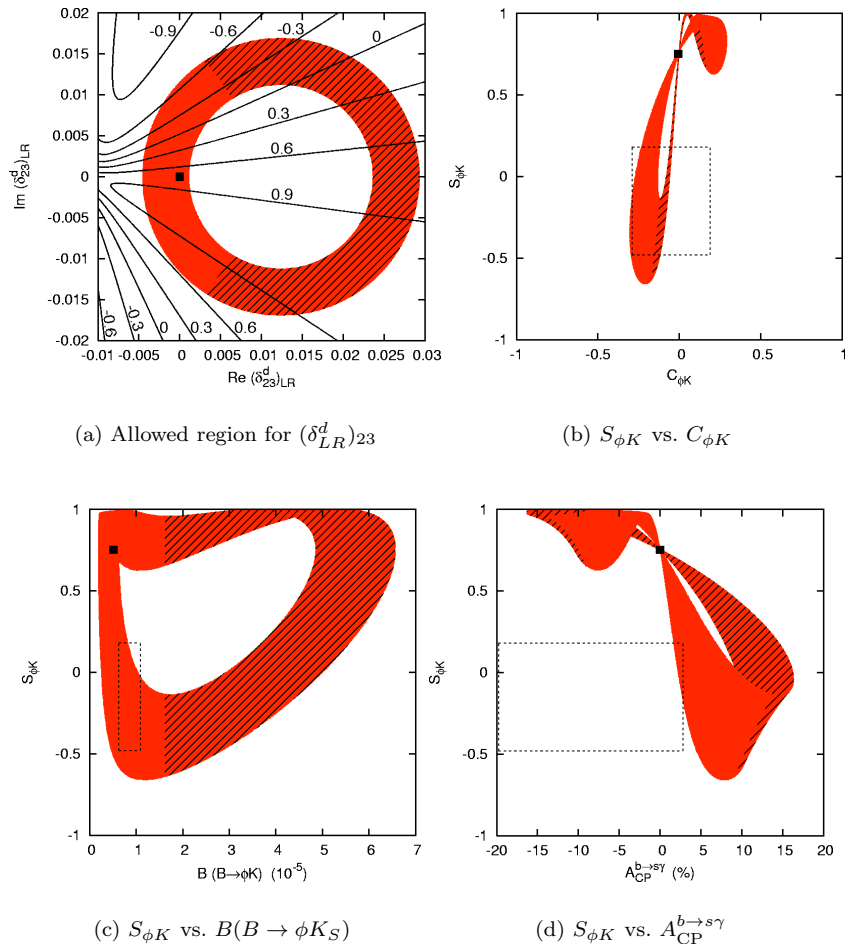


FIG. 3: (a) Allowed region on the complex plane of  $(\delta_{LR}^d)_{23}$ , and (b–d) correlations among observables for the  $LR$  insertion case. The black square corresponds to the SM case. The dotted boxes represent current measurements at  $1\text{-}\sigma$  level. Lines in Fig. (a) are contours of  $S_{\phi K}$ .

when they contribute to a (chromo) magnetic dipole operator. This is why they are strongly constrained by  $B \rightarrow X_s \gamma$ . For the same reason, they are more effective in modifying  $S_{\phi K}$  and/or  $C_{\phi K}$  than  $LL$  or  $RR$  insertion given the same magnitude of the MI parameter. We show the region of  $(\delta_{LR}^d)_{23}$  consistent with  $B(B \rightarrow X_s \gamma)$  and  $\Delta M_s$  in Fig. 3 (a). As in the previous case, the solid lines are contours of  $S_{\phi K}$ , and the small square at the origin corresponds to the SM case. The annulus with radius  $\sim 10^{-2}$  comes from the  $B(B \rightarrow X_s \gamma)$ . Here the  $B(B \rightarrow X_s \gamma)$  constraint is so strong that  $\Delta M_s$  does not change very much from the SM value and play no role in constraining  $(\delta_{LR}^d)_{23}$ . We show  $S_{\phi K}$  and  $C_{\phi K}$  from these values of  $(\delta_{LR}^d)_{23}$  in Fig. 3 (b). The dotted box is  $1\text{-}\sigma$  intervals of these observables, and we find some region where both  $S_{\phi K}$  and  $C_{\phi K}$  are within the box. This plot also shows a definite correlation between them. For  $S_{\phi K}$  less (bigger) than the SM value,  $C_{\phi K} < (>) 0$ . Fig. 3 (c) is the plot of  $B(B \rightarrow \phi K_S)$ , with hatches on the region

where  $B(B \rightarrow \phi K_S) > 1.6 \times 10^{-5}$ . This region, excluded by  $B(B \rightarrow \phi K_S)$  constraint, corresponds to the hatched region in Fig. 3 (a). Here we learn that significant portion of the  $(\delta_{LR}^d)_{23}$  parameter space that is consistent with  $B(B \rightarrow X_s \gamma)$ , is excluded by  $B(B \rightarrow \phi K_S)$ . In Fig. 3 (d) is displayed the correlation between  $S_{\phi K}$  and direct  $CP$  asymmetry in  $B \rightarrow X_s \gamma$ . For  $S_{\phi K}$  less (bigger) than the SM value,  $A_{CP}^{b \rightarrow s \gamma} > (<) 0$ . It appears that  $A_{CP}^{b \rightarrow s \gamma}$  is outside the dotted box, but the experimental uncertainty is still large, so we cannot definitely conclude that this scenario is disfavored currently.

We turn to the  $RL$  dominance scenario. Fig. 4 (a) is the region of  $(\delta_{RL}^d)_{23}$  constrained by  $B(B \rightarrow X_s \gamma)$  and  $\Delta M_s$ . Again, the solid lines are contours of  $S_{\phi K}$ . In this case, we are assuming that SM contributions to  $C_{7\gamma}$  and  $C_{8g}$  are somehow canceled by SUSY contributions. Because we are always involving SUSY contributions in  $C_{7\gamma}$  and  $C_{8g}$ , there cannot be any point on the  $(\delta_{RL}^d)_{23}$  plane that reduces to the SM case. The allowed annulus,

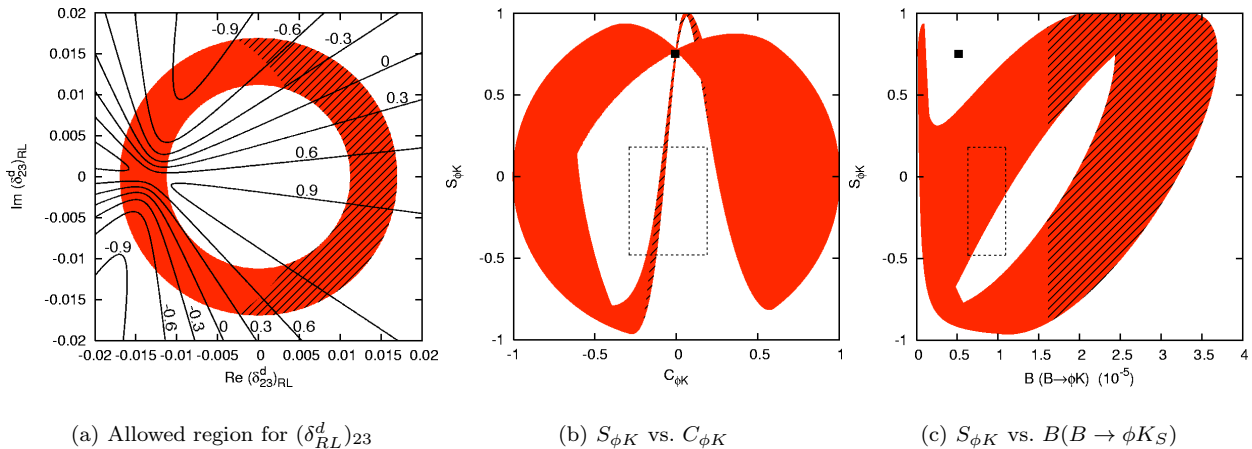


FIG. 4: (a) Allowed region on the complex plane of  $(\delta_{RL}^d)_{23}$ , and (b–c) correlations among observables for the  $RL$  dominance case. The black square corresponds to the SM case. The dotted boxes represent current measurements at  $1\text{-}\sigma$  level. Lines in Fig. (a) are contours of  $S_{\phi K}$ .

centered at the origin, has radius  $\sim 10^{-2}$ , which is fixed by  $B(B \rightarrow X_s \gamma)$ . As in the previous case, the region consistent with  $B(B \rightarrow X_s \gamma)$  is always consistent with  $\Delta M_s$  as well. Predictions of  $S_{\phi K}$  and  $C_{\phi K}$  from the allowed region are shown in Fig. 4 (b). We can fit  $S_{\phi K}$  to any value between  $-1$  and  $1$ . Moreover, big change in  $C_{\phi K}$  from the SM value of zero, is expected in general, resulting in any value between  $-1$  and  $1$ . However, some region around the center is not covered. In Fig. 4 (c), we plot  $B(B \rightarrow \phi K_S)$ , with hatches on the region with excessive  $B(B \rightarrow \phi K_S)$ . Since there is only one weak phase in the  $b \rightarrow s \gamma$  amplitude, we have  $A_{\text{CP}}^{b \rightarrow s \gamma} = 0$  in this case. If we turned on another weak phase such as coming from  $(\delta_{RR}^d)_{23}$ , we could have non-vanishing  $A_{\text{CP}}^{b \rightarrow s \gamma}$ , but we do not pursue more detailed analysis here.

We also analyzed the usual  $RL$  insertion case, keeping SM contributions to  $C_{7\gamma}$  and  $C_{8g}$ . Because the SM prediction of  $B(B \rightarrow X_s \gamma)$  is already consistent with the data, there is less room for new physics in this case than in the  $RL$  dominance scenario. Nevertheless, we can get sizable change in  $S_{\phi K}$ , satisfying  $B(B \rightarrow X_s \gamma)$ . Plots for this case can be found in Ref. [6].

These results of analysis depend on the sparticle mass scale. For a fixed value of MI parameter, SUSY effects get enhanced as the sparticle masses decrease. In Figs. 5, we show possible values of  $S_{\phi K}$  as functions of the gluino mass,  $m_{\tilde{g}}$ . In these plots, we fix the ratio  $x \equiv m_{\tilde{g}}^2/\tilde{m}^2$  to be 1, and scan over one of the four MI parameters imposing constraints from  $B(B \rightarrow X_s \gamma)$  and  $\Delta M_s$ . Figs. 5 (a) and (b) are for the chirality-preserving insertions,  $LL$  and  $RR$ , respectively. Here we see a clear tendency of SUSY effects decoupling as the gluino mass increases. Note that our analysis shown in Figs. 2–4 is for  $m_{\tilde{g}} = 400$  GeV. The way to getting  $S_{\phi K}$  consistent with the data is to imagine the gluino mass  $\sim 250$  GeV, which is close

to the current experimental lower bound. On the other hand, a chirality-flipping insertion,  $LR$  or  $RL$ , shown in Figs. 5 (c) and (d), results in a range of  $S_{\phi K}$  that is independent of  $m_{\tilde{g}}$ . This is explained in the following way in the  $LR$  insertion case for example. The dependence of  $B \rightarrow X_s \gamma$  on the SUSY parameters is only through the ratio of  $(\delta_{LR}^d)_{23}/m_{\tilde{g}}$ , which precisely is the parameter that  $S_{\phi K}$  also depends on. The set of  $(\delta_{LR}^d)_{23}/m_{\tilde{g}}$  allowed by  $B(B \rightarrow X_s \gamma)$  is independent of  $m_{\tilde{g}}$ , and so is  $S_{\phi K}$ . The  $RL$  and  $RR$  dominance cases are explained likewise. In fact, this type of constant dependence would be true for  $LL$  or  $RR$  insertion case as well, if we allowed arbitrarily large size of  $(\delta_{LL}^d)_{23}$  or  $(\delta_{RR}^d)_{23}$  and if we discarded  $\Delta M_s$  constraint.

In the QCD factorization, divergences coming from endpoint of integral  $\int dx/x$  are regulated in the form of  $X_{A(H)} = (1 + \varrho_{A(H)} e^{i\varphi_{A(H)}}) \ln(m_B/\Lambda_h)$ , where  $\Lambda_h \sim 0.5$  GeV is the scale in hard-scattering. Discussion so far has been carried out without considering any uncertainties coming from this regularization, but we have to scan over the parameters  $\varrho_{A,H}$  and  $\varphi_{A,H}$  properly to take care of these theoretical uncertainties. In Fig. 6 (a), we show a curve of  $S_{\phi K}$  as a function of the gluino mass. In this plot, we fix  $x = 1$ , and turn on only the  $RR$  insertion with the value  $(\delta_{23}^d)_{RR} = 0.534 - 0.856i$ , which minimizes  $S_{\phi K}$  at  $m_{\tilde{g}} = 200$  GeV. This curve is broadened into bands shown in Fig. 6 (b), if we begin to scan over the aforementioned parameters. In general, the uncertainty in the annihilation from  $\varrho_A$  dominates over that in hard spectator scattering from  $\varrho_H$ . The black band is for the range  $0 \leq \varrho_A, \varrho_H \leq 1$ , and this is what the authors of Ref. [5] recommend to use. On this band, the tendency of decoupling SUSY effects with increasing  $m_{\tilde{g}}$  is still maintained. However, for the case of  $0 \leq \varrho_A, \varrho_H \leq 5$ , which is displayed in light gray, estimated theoretical uncertainties

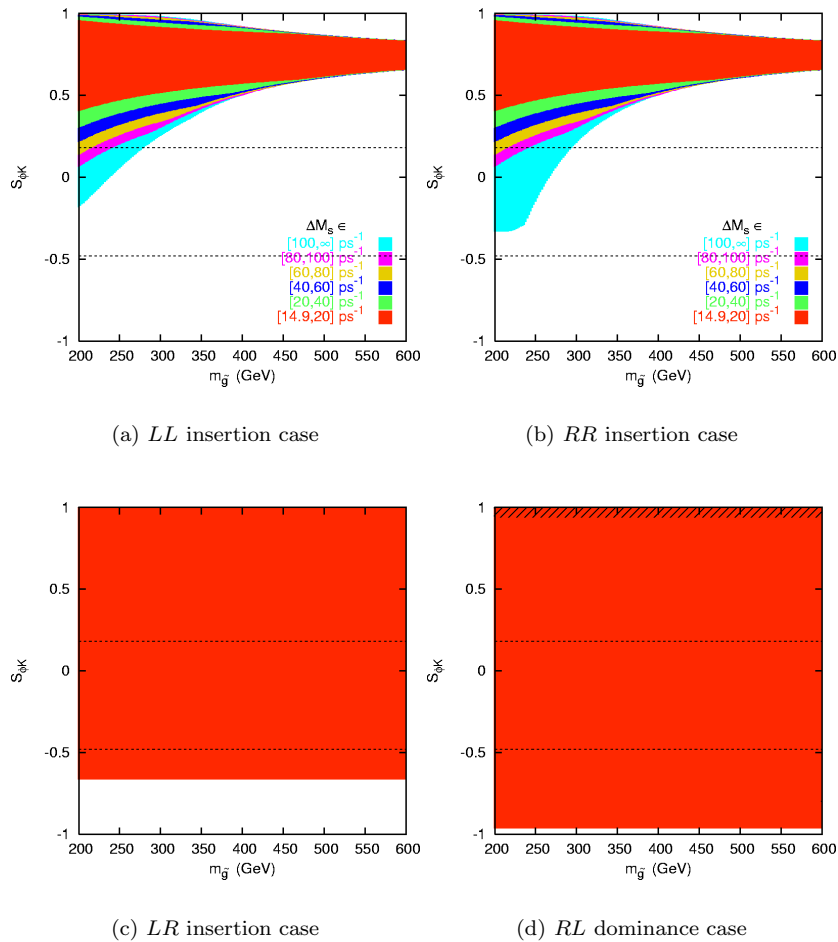


FIG. 5: Possible range of  $S_{\phi K}$  as a function of the gluino mass. Different shades are used for different values of  $\Delta M_s$ . The dotted lines represent the current bounds on  $S_{\phi K}$  at  $1\text{-}\sigma$  level.

are so large that almost every value of  $S_{\phi K}$  between  $-1$  and  $1$  is predicted, for any gluino mass between  $200$  GeV and  $600$  GeV. Ref. [7] claims that they get  $S_{\phi K} < 0$  from *LL* or *RR* insertion with  $m_{\tilde{g}} = 350$  GeV, disagreeing with us. We suspect this is due to the difference in choosing intervals for  $\varrho_A$  and  $\varrho_H$ . They use  $0 \leq \varrho_A \leq 8$ , and from Fig. 6 (b), it is obvious that  $S_{\phi K}$  will have every value between  $-1$  and  $1$  for this interval.

Let us think of theoretical motivations for  $(\delta_{LR}^d)_{23}$  or  $(\delta_{LR}^d)_{23} \sim 10^{-2}$ . In many alignment models using flavor symmetry, there remain small off-diagonal elements in the squark mass matrix in the super CKM basis. They can cause  $(\delta_{23}^d)_{LL}$  or  $(\delta_{23}^d)_{RR} \sim 10^{-2}$  with arbitrary complex phase. This chirality preserving insertion can lead to an induced *LR* or *RL* insertion,

$$(\delta_{LR}^d)_{23}^{\text{ind}} = (\delta_{LL}^d)_{23} \times \frac{m_b(A_b - \mu \tan \beta)}{\tilde{m}^2} \sim 10^{-2},$$

provided  $\tan \beta$  is large enough so that  $\mu \tan \beta \sim 30$  TeV. This kind of double insertion mechanism has been used in explaining both  $\epsilon_K$  and  $\epsilon'/\epsilon_K$  from a single *CP* violation

source of  $(\delta_{LL}^d)_{12}$  [8]. We also constructed a model that naturally gives the desired amount of *LR* or *RL* insertion using intersecting D5 branes [6].

Since QCD penguin contributes to  $b \rightarrow s\bar{q}q$  for  $q = u, d, s, c, b$  at equal strength, one may worry about what happens to other decays such as  $B \rightarrow \eta' K_S, \pi K, K^+ K^- K_S$ . There are other 4-quark operators which contribute only to these decays not affecting  $B \rightarrow \phi K_S$ , and changes in these decay modes are not definitely predictable in the present study. On the other hand, there is a nice mechanism which enables us to control  $B \rightarrow VP$  and  $B \rightarrow PP$  modes independently. Parity invariance tells us that the transition amplitudes of these modes depend on the new physics contribution in such a way that  $B \rightarrow VP$  (*PP*) mode depends on  $\sum_i [C_i^{\text{NP}} + (-) \tilde{C}_i^{\text{NP}}] \#_i$ , where  $C_i^{\text{NP}}$  and  $\tilde{C}_i^{\text{NP}}$  are Wilson coefficients with opposite chiralities, coming from new physics. Hence we can control  $B \rightarrow \eta' K_S$  and  $B \rightarrow \phi K_S$  separately, and only the latter will change if we imagine a situation where  $(\delta_{LR}^d)_{23} = (\delta_{RL}^d)_{23}$ , for instance. If this

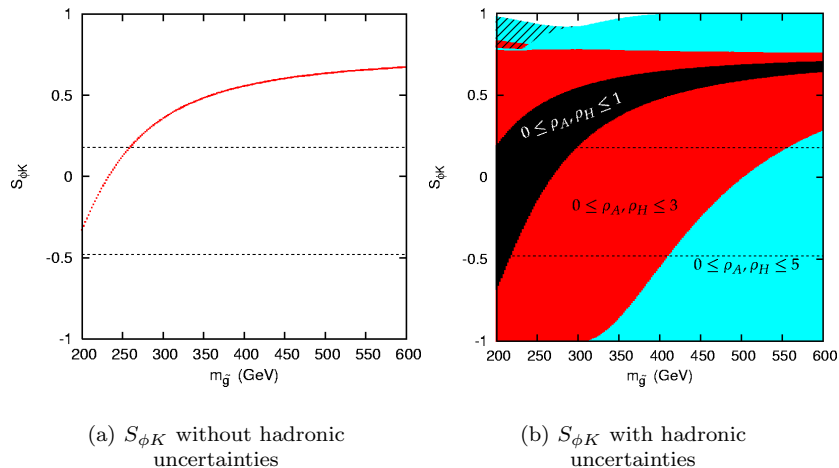


FIG. 6: Predictions of  $S_{\phi K}$  from  $(\delta_{23}^d)_{RR} = 0.534 - 0.856i$  as functions of the gluino mass, (a) with  $X_A = X_H = 0$ , and (b) with varying  $\rho_A, \rho_H$ . The dotted lines represent the current bounds on  $S_{\phi K}$  at 1- $\sigma$  level. In Fig. (b), different shades are used for different ranges of  $\rho_A$  and  $\rho_H$ .

is the case, predictions of other observables such as  $C_{\phi K}$  and  $A_{\text{CP}}^{b \rightarrow s \gamma}$  will be different than the four cases we considered here. After all, it requires further study to see changes in other decay modes in more general cases.

From now, we consider the neutral Higgs mediated contribution to  $B \rightarrow \phi K_S$ . A typical diagram is shown in Fig. 7. This diagram contributes to  $B_s \rightarrow \mu^+ \mu^-$

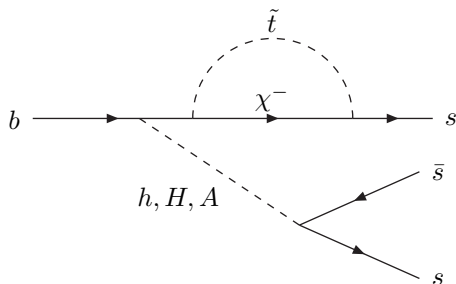


FIG. 7: Higgs penguin diagram.

as well as to  $B \rightarrow \phi K_S$  if we replace the  $s\bar{s}$  pair with  $\mu^+ \mu^-$ . Once we impose the upper bound from CDF [9],  $B(B_s \rightarrow \mu^+ \mu^-) < 2.6 \times 10^{-6}$ , we find that  $S_{\phi K} > 0.71$ . This argument applies not only in minimal flavor violation scenario, but also in general MSSM [6]. As a result, Higgs exchange does not cause substantial change in  $S_{\phi K}$ .

In conclusion, we analyzed SUSY contributions to time dependent  $CP$  asymmetry in  $B \rightarrow \phi K_S$ . As to the gluino-squark loop, negative  $S_{\phi K}$  is more likely to come from  $LR$  or  $RL$  insertion than from  $LL$  or  $RR$  insertion if the sparticle masses are not close to the current experimental lower bound. However, we may have chances to look for  $LL$  or  $RR$  insertion in  $B_s - \bar{B}_s$  mixing. Correlations among  $S_{\phi K}$ ,  $C_{\phi K}$ ,  $A_{\text{CP}}^{b \rightarrow s \gamma}$ ,  $\Delta M_s$ ,  $\sin 2\beta_s$  may help

us discriminate among different possibilities. Constraint from nonleptonic decays such as  $B \rightarrow \phi K_S$  is becoming as severe as that from  $B \rightarrow X_s \gamma$ . Higgs mediated FCNC cannot explain  $S_{\phi K} < 0$ . Finally, let us direct the reader to Ref. [6] for more complete discussion including dilepton  $CP$  asymmetry in  $\Upsilon(4S)$  decay.

The author is grateful to G. L. Kane, P. Ko, C. Kolda, Haibin Wang, and Lian-Tao Wang, for enjoyable collaboration. This work was supported in part by KOSEF through CHEP at Kyungpook National University and by the BK21 program.

<sup>†</sup> jhpark@particle.kaist.ac.kr

- [1] T. Browder, talk at Lepton Photon 2003, Fermilab, Aug. 11-16, 2003.
- [2] K. Abe *et al.* [Belle Collaboration], hep-ex/0308035.
- [3] L. Everett, G. L. Kane, S. Rigolin, L. T. Wang and T. T. Wang, JHEP **0201**, 022 (2002).
- [4] A. Stocchi, hep-ph/0010222.
- [5] M. Beneke, G. Buchalla, M. Neubert and C. T. Sachrajda, Phys. Rev. Lett. **83**, 1914 (1999); Nucl. Phys. B **591**, 313 (2000); Nucl. Phys. B **606**, 245 (2001).
- [6] G. L. Kane, P. Ko, H. b. Wang, C. Kolda, J.-h. Park and L. T. Wang, hep-ph/0212092; Phys. Rev. Lett. **90**, 141803 (2003).
- [7] M. Ciuchini, E. Franco, A. Masiero and L. Silvestrini, Phys. Rev. D **67**, 075016 (2003) [Erratum-ibid. D **68**, 079901 (2003)].
- [8] S. Baek, J. H. Jang, P. Ko and J.-h. Park, Phys. Rev. D **62**, 117701 (2000); Nucl. Phys. B **609**, 442 (2001).
- [9] F. Abe *et al.* [CDF Collaboration], Phys. Rev. D **57**, 3811 (1998).